

# The Crystal Structure of a Mammalian Fatty Acid Synthase

Timm Maier, Marc Leibundgut, Nenad Ban\*

Mammalian fatty acid synthase is a large multienzyme that catalyzes all steps of fatty acid synthesis. We have determined its crystal structure at 3.2 angstrom resolution covering five catalytic domains, whereas the flexibly tethered terminal acyl carrier protein and thioesterase domains remain unresolved. The structure reveals a complex architecture of alternating linkers and enzymatic domains. Substrate shuttling is facilitated by flexible tethering of the acyl carrier protein domain and by the limited contact between the condensing and modifying portions of the multienzyme, which are mainly connected by linkers rather than direct interaction. The structure identifies two additional nonenzymatic domains: (i) a pseudo-ketoreductase and (ii) a peripheral pseudo-methyltransferase that is probably a remnant of an ancestral methyltransferase domain maintained in some related polyketide synthases. The structural comparison of mammalian fatty acid synthase with modular polyketide synthases shows how their segmental construction allows the variation of domain composition to achieve diverse product synthesis.

Fatty acids fulfill a variety of vital functions: They are central constituents of biological membranes, serve as energy storage compounds, and act as second messengers or as covalent modifiers governing the localization of proteins. In bacteria and plants, fatty acid biosynthesis is accomplished by a series of monofunctional proteins in a dissociated type II fatty acid synthase (FAS) system (1). In contrast, the type I FASs of fungi and animals are huge multifunctional polypeptides that integrate all steps of fatty acid synthesis into large macromolecular assemblies. Fungal FAS is a 2.6-MD  $\alpha_6\beta_6$ -heterododecamer with the catalytic domains distributed over two polypeptides (2–4), whereas mammalian FAS (mFAS) consists of a 270-kD polypeptide chain (comprising all seven required domains) that assembles into homodimers for enzymatic activity (5, 6).

Despite this variation in structural organization, all organisms employ a conserved set of chemical reactions for fatty acid biosynthesis (1, 6–8). Stepwise elongation of precursors is achieved by cyclic decarboxylative condensation of acyl-coenzyme A (CoA) with the elongation substrate malonyl-CoA, initiated by the starter substrate acetyl-CoA. In the priming step, the acetyl transferase loads acetyl-CoA onto the terminal thiol of the phosphopantetheine cofactor of the acyl carrier protein (ACP), which passes the acetyl moiety over to the active site cysteine of the  $\beta$ -ketoacyl synthase (KS). Malonyl transferase (MT) transfers the malonyl group of malonyl-CoA to ACP, and the KS catalyzes the decarboxylative condensation of the acetyl and malonyl moieties to an ACP-bound  $\beta$ -ketoacyl

intermediate. The  $\beta$ -carbon position is then modified by sequential action of the NADPH (the reduced form of nicotinamide adenine dinucleotide, NADP<sup>+</sup>)-dependent  $\beta$ -ketoreductase (KR), a dehydratase (DH), and the NADPH-dependent enoyl reductase (ER) to yield a saturated acyl product elongated by two carbon units. This acyl group functions as a starter substrate for the next round of elongation, until the growing fatty acid chain reaches a length of 16 to 18 carbon atoms and is released from ACP. In mFAS, the malonyl and acetyl transferase reactions are catalyzed by a single bifunctional protein domain, the malonyl-acetyl transferase (MAT), and the products are released from ACP as free fatty acids by a thioesterase (TE) domain (6).

Humans eating a typical Western diet take in a surplus of fatty acids. Consequently, de novo fatty acid biosynthesis and FAS activity are low in most body tissues. However, FAS is overexpressed in many cancer cells, and its expression level is correlated with tumor malignancy (9). FAS inhibitors have demonstrated anti-tumor activity in vivo and in vitro, and in recent years FAS has emerged as an important drug target for the treatment of human cancer (10, 11). The medical use of FAS inhibitors has been hampered by off-target activities. Recently, more specific inhibitors of type I FAS have been described (12) and remain to be tested.

Currently, high-resolution structures are known for all components of bacterial (1) and fungal FAS (2, 4, 13), whereas the structural information for mFAS is limited to high-resolution structures for the isolated MAT [Protein Data Bank (PDB) entry 2jfd], ACP (14, 15), and TE domains (16, 17) and a domain architecture model based on a 4.5 Å resolution x-ray crystallographic map (5). Structure determination of KS-acyl transferase didomain fragments and KR domains of polyketide synthases (PKS) (18–21)—large

modular megasynthases involved in the microbial synthesis of a number of bioactive compounds and drugs—has confirmed the anticipated close structural relation between mFAS and PKS modules (6, 22). Here, we present the crystal structure of mFAS in its free and NADP<sup>+</sup>-bound states, in which the flexibly tethered C-terminal ACP/TE domains (23) remain unresolved.

## Overall Structure and Topology

The crystal structures of natively purified mFAS from pigs, free and in complex with the cofactor NADP<sup>+</sup>, have been determined at 3.2 and 3.3 Å resolution and refined to  $R/R_{\text{free}}$  values of 0.22/0.26 and 0.19/0.24, respectively (where  $R/R_{\text{free}}$  are  $\Sigma|F_{\text{obs}}(h) - F_{\text{calc}}(h)|/\Sigma F_{\text{obs}}(h)$  calculated for the working/test set of reflections). Diffraction data were affected by anisotropy with one weaker direction of reciprocal space (24). mFAS assembles into an intertwined dimer approximating an “X” shape (Fig. 1A). This structure agrees well with our previous architectural model at intermediate resolution (5) and additionally provides the connectivities of domains, the detailed features of active sites, and the nature of linking sequences outside the conserved core domains. mFAS is segregated into a lower condensing portion, containing the condensing KS and the MAT domains, and an upper portion including the DH, ER, and KR domains responsible for  $\beta$ -carbon modification (Fig. 1, A and B). Two additional nonenzymatic domains are located at the periphery of the modifying part. The first of these domains is homologous to the methyltransferase family and is thus named “pseudo-methyltransferase” ( $\Psi$ ME). The second represents a truncated KR fold dimerizing with the catalytic KR domain and is referred to as “pseudo-ketoreductase” ( $\Psi$ KR). The condensing and modifying parts of mFAS are loosely connected and form only tangential contacts. The structural organization of domains deviates dramatically from their linear arrangement in sequence (Fig. 1, A and C).

The two polypeptides dimerize through an extended contact area of 5400 Å<sup>2</sup>, which involves more than 150 residues per chain (table S2). The main contributions to this interface arise from homophilic interactions of the KS and ER domains, with areas of ~2600 and 1600 Å<sup>2</sup>, which resemble the dimer organization of monofunctional homologs (25, 26). Additional dimer contacts (800 Å<sup>2</sup>) are provided by the DH domain through homophilic interactions between the double “hot dog” folds via a loop around residue 941. The remaining interactions are formed by the C-terminal part of the linker region between the MAT and DH domains (residues 846 to 860) with the KS domain of the other chain (400 Å<sup>2</sup>).

## Interdomain Linking and Interaction

The characteristics of multienzyme complexes are to a great degree determined by the nature of

Institute of Molecular Biology and Biophysics, ETH Zurich, 8092 Zurich, Switzerland.

\*To whom correspondence should be addressed. E-mail: ban@mol.biol.ethz.ch

the interactions and linking of functional subunits. Notably, animal FAS invests only ~9% of its total sequence for linkers (Fig. 2, A to E) and an additional 16% for the lateral noncatalytic  $\Psi$ ME and  $\Psi$ KR domains (Fig. 1A). No scaffolding insertions are found in the catalytic cores. This is in contrast to the fungal FAS, the other megasynthase for which a high-resolution structure is available (2, 4, 13). In that multienzyme, almost 50% of the total sequence forms a complex structural matrix of numerous inter- and intradomain insertions, which define the spatial organization of the catalytic domains. The only structured linker domain in mFAS connects the KS and MAT domains [KS-MAT linker domain (Fig. 2A)] and is composed of amino acids 420 to 490 between KS and MAT and of residues 809 to 837 joining MAT and DH. It includes two short  $\alpha$ -helices facing the KS and a three-stranded antiparallel  $\beta$  sheet on the MAT side and acts as an adapter, preventing any direct interaction between the KS and MAT domains. Similar linker domains were recently found in the KS-acyl transferase didomain structures of two PKS modules (18, 21). Although an additional helix is inserted in the PKS linker domains (fig. S1), the relative positions of the transferase and KS domains remain essentially the same in mFAS and PKS (fig. S2).

The connection between the condensing and modifying part of mFAS is provided by residues 838 to 858 between the KS-MAT linker domain and the DH domain (Fig. 2, D and E). Again, the conformation and position of this linker closely resembles those observed in KS-acyl transferase didomain structures from PKS modules, even though these didomains are derived from modules with a considerably different sequence context, containing only KR domains for  $\beta$ -carbon modification (18, 21). Besides the linker itself, only very limited contacts are formed between the condensing and modifying parts of mFAS (with an interaction area of 230  $\text{\AA}^2$ ). It is even possible that some percentage of molecules in the crystal have an alternative connectivity between the two parts (equivalent to a rotation of the upper portion of the molecule), which would escape detection by crystallographic methods (figs. S3 and S4).

The KR domain acts as a central connector for the modifying part of mFAS and interacts with the DH, ER, and noncatalytic  $\Psi$ ME and  $\Psi$ KR domains (Fig. 3, A and B, and table S3). In contrast, neither the DH nor the ER domain interacts with either of the noncatalytic domains, and the contact between the DH and ER domains is very weak. The KR domain interacts with the

second hot dog subdomain of DH, forming an 800  $\text{\AA}^2$  interface. The contact between KR and ER is less intricate and extends over an area of 400  $\text{\AA}^2$ . About 10% (or 1100  $\text{\AA}^2$ ) of the KR surface is involved in a contact with the  $\Psi$ KR domain, mimicking one of the two major dimerization interfaces observed in the tetrameric KR of bacteria (fig. S5). The  $\Psi$ ME, which has the highest mobility based on atomic displacement parameter analysis (fig. S6), protrudes from the mostly planar body of mFAS. It is docked via interactions with the KR and the  $\Psi$ KR domain, the former providing 20% (200  $\text{\AA}^2$ ) and the latter 80% (800  $\text{\AA}^2$ ) of the docking area.

Most of the linker regions in the modifying domains are solvent exposed (Fig. 2). An important exception is  $\beta$  strand-forming regions at the N terminus of the  $\Psi$ KR-ER linker (residues 1513 to 1518) and the C terminus of the DH2- $\Psi$ ME linker (residues 1117 to 1123). These are buried between the KR,  $\Psi$ KR, and  $\Psi$ ME domains and have an important structural role, as discussed in the next paragraph (Fig. 2C).

### The Nonenzymatic Domains

The KR character of the mFAS  $\Psi$ KR domain, which has approximately half the size of the active KR domain, is maintained only in the

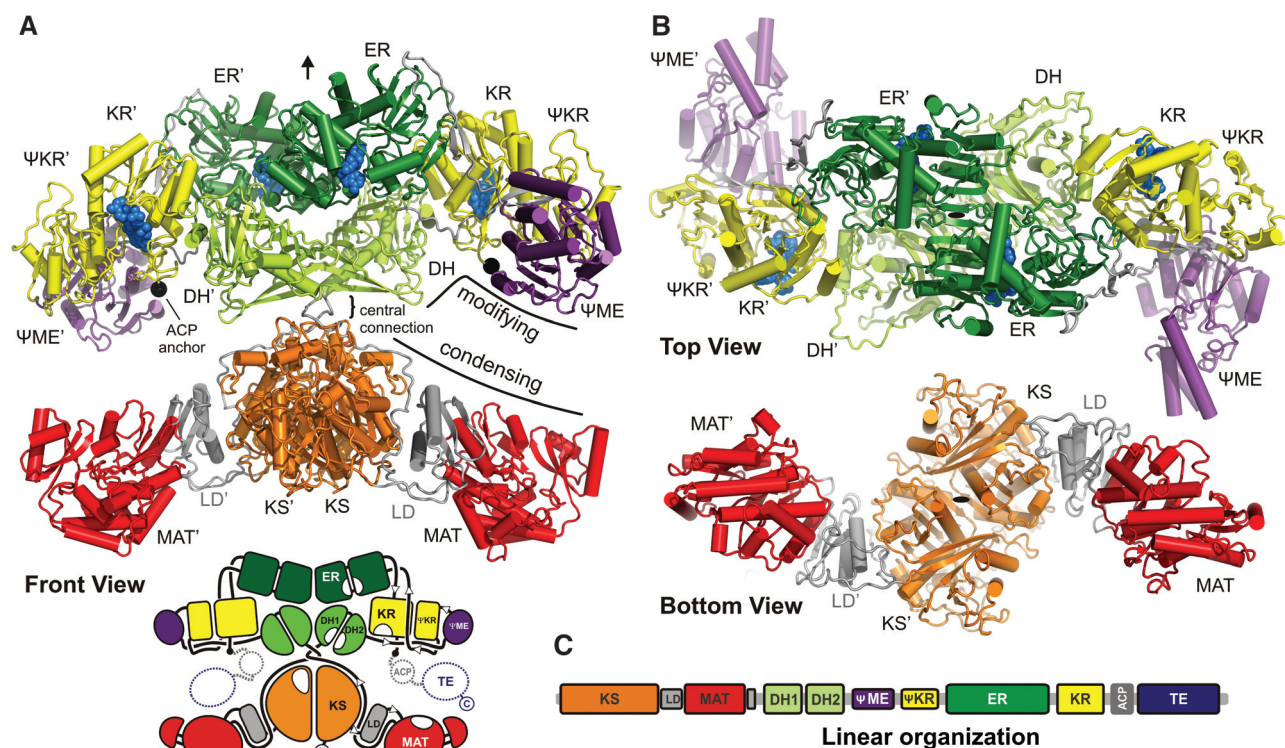


**Fig. 1.** Structural overview. **(A)** Cartoon representation of mFAS, colored by domains as indicated. Linkers and linker domains are depicted in gray. Bound  $\text{NADP}^+$  cofactors and the attachment sites for the disordered C-terminal ACP/TE domains are shown as blue and black spheres, respectively. The position of the pseudo-twofold dimer axis is depicted by an arrow; domains of the second chain are indicated by an appended

prime. The lower panel (front view) shows a corresponding schematic diagram. **(B)** Top (upper panel) and bottom (lower panel) views, demonstrating the “S” shape of the modifying (upper) and condensing (lower) parts of mFAS. The pseudo-twofold axis is indicated by an ellipsoid. **(C)** Linear sequence organization of mFAS, at approximate sequence scale.

conserved dimerization interface. Because of extensive truncation of its core, it has lost the ability to bind NADPH. Consequently, the  $\Psi$ KR domain functions mainly to support the integrity of the active site of the catalytic KR domain. The KR/ $\Psi$ KR arrangement closely resembles the structure of a KR- $\Psi$ KR domain derived from 6-deoxyerythronolide B synthase (DEBS) PKS module 1 (19) (Fig. 3A). The mFAS  $\Psi$ KR domain lacks the two N-terminal sheet-helix windings of the DEBS1  $\Psi$ KR, which itself is already shorter than the catalytically active KR fold (Fig. 3A). Because of the insertion of the ER and  $\Psi$ ME domains into the KR- $\Psi$ KR fold, two  $\beta$  strands originally formed by the linkers flanking the KR and  $\Psi$ KR domains are no longer directly adjacent to these two domains in the mFAS sequence. Rather, they are provided by amino acid stretches leading from the DH2 into the  $\Psi$ ME domain, 300 amino acids upstream of the  $\Psi$ KR, and the linker between  $\Psi$ KR and ER, separated by 360 residues from the KR domain (Fig. 3C).

The  $\Psi$ ME domain is structurally closely related to *S*-adenosyl-methionine (SAM)-dependent methyltransferases, in spite of low sequence ho-

mology (fig. S7A and table S4). The core of these enzymes consists of a seven-stranded  $\beta$  sheet with three helices on each side and the C-terminal strand in anti-parallel orientation (27). The methyltransferase fold of mFAS carries an additional short  $\beta$  strand and three helices at its N terminus (residues 1125 to 1224). At its C terminus, a short linker (residues 1407 to 1413) leads directly into the adjacent  $\Psi$ KR fold. Such a topology is characteristic of small-molecule (including lipid) methyltransferases (27). Nevertheless, the D/ExGxGxG motif involved in SAM cofactor binding (27) is not conserved in any of the metazoan FAS sequenced so far (fig. S8). In FAS of mammals, this motif is changed to ExLxGxG, which probably prevents cofactor binding, in agreement with the absence of methyltransferase activity and methylated products in mFAS systems. Notably, this motif is strictly conserved in several iterative and modular PKSs found in fungi and bacteria that share a related overall domain organization with FAS but are able to methylate their polyketide substrate with an intrinsic C-methyltransferase activity (fig. S7B) (28–30). Thus, the  $\Psi$ ME domain of FAS most likely represents an inactive version of a previously

functional enzyme in a common precursor of mFAS and PKSs.

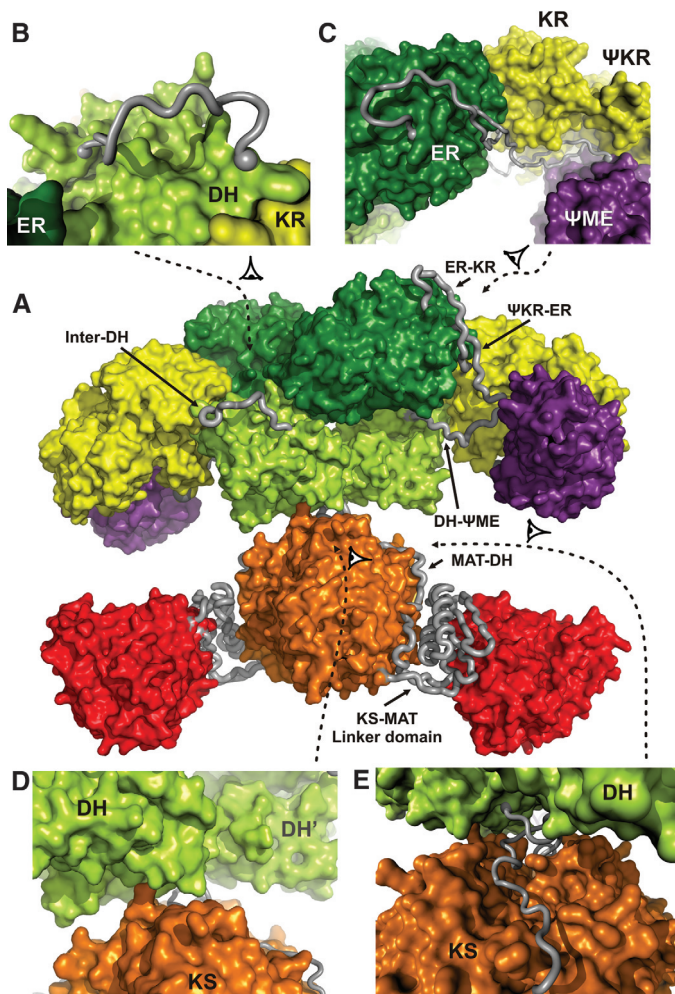
### Catalytic Domains and Cofactor Binding

**Ketoacyl synthase.** The KS enzymes of all systems for fatty acid or modular polyketide synthesis share a common fold and chemical mechanism, but their substrate specificities differ considerably (1, 6). In the bacterial systems, which lack an acetyltransferase, KASIII (FabH) directly accepts acetyl-CoA as starter substrate. Further acyl chain extensions from C4 to C14 and from C14 to C16 are carried out by KASI (FabB) and KASII (FabF), respectively. Modular PKS contain specialized KS with some specificity for the  $\beta$ -carbon status but accept a wide range of substrate lengths (6). In the fungal type I FAS, only a single KS (which accepts C2 to C16 primers) is required for fatty acid synthesis. Likewise, mFAS has a single KS domain for all steps of fatty acid elongation. In contrast to PKS KS, mFAS KS is highly specific for saturated acyl chains and does not accept  $\beta$ -ketoacyl,  $\beta$ -enoyl- or  $\beta$ -hydroxyacyl substrates (6, 31). On the basis of structural alignments, mFAS KS is closely related to KS domains from the DEBS I PKS system [1.3 Å root mean square deviation (RMSD)] but is structurally also very similar to fungal KS (RMSD 1.8 Å). It is more closely related to bacterial KASI and KASII (1.8 Å/1.6 Å RMSD) than to KASIII (2.9 Å RMSD), reflecting its ability to elongate long ACP-bound acyl chains.

Despite the pronounced structural similarity between the KS domains of mFAS and PKS, the selectivity of FAS for saturated acyl chains can be explained by a considerable constriction at the base of the active site phosphopantetheine binding pocket leading into the large acyl chain substrate binding tunnel, which connects both active sites of the KS dimer (Fig. 4, A and B). A number of residues lining this narrow tunnel are highly conserved in mFAS but are substituted with smaller residues in all DEBS PKS modules (Fig. 4B), resulting in a wider, more permissive tunnel in the KS of DEBS.

**Malonyl-acetyl transferase.** The acyl transferases of FAS and PKS systems are composed of an  $\alpha/\beta$ -hydrolase core fold and a ferredoxin-like subdomain, which together create the active site cleft (32). In mFAS, the MAT domains of the two monomers have slightly different relative orientations of the two subdomains, probably selected by crystal-packing interactions. The structurally closest relatives are acyl transferases from DEBS didomain structures (2.0 Å/2.2 Å RMSD), the human mitochondrial MT (2.2 Å), and the *Escherichia coli* FAS MT (FabD) (2.3 Å RMSD) (table S4). All members of this family share a conserved active site with a catalytic Ser-His dyad. MTs are distinguished from acetyl transferases by the presence of a conserved active site arginine (2), which forms a bidentate salt bridge with the malonyl carboxylate (33). The mFAS MAT and related MTs display a rather

**Fig. 2.** Interdomain linkers. (A) Surface representation of individual mFAS domains (front view), colored as in Fig. 1. Linking regions are shown as tubes. (B to E) Close-up views of individual linkers. The direction of view is indicated by arrowheads in (A). (B) Linker connecting the two subdomains of the DH domain only loosely interacts with the main body of the double hot dog fold. (C) Linkers in the KR/ER region are wrapped around the domains with close interactions to the domain surfaces and pronounced linker-linker contacts; they mediate interactions between the KR,  $\Psi$ KR, and  $\Psi$ ME domains. (D) Modifying upper and condensing lower parts of FAS are only in tangential contact in the region of the central connection. Few residues besides the connecting linkers mediate the sparse interactions via a small interface area. (E) MAT-DH linker meanders through a groove on the surface of the KS domain.



broad specificity for malonyl-CoA derivatives (e.g., propionyl-CoA and methylmalonyl-CoA). However, only mFAS MAT uses both acetyl-CoA and malonyl-CoA with equal efficiency (6). A structural comparison with bacterial and PKS MTs reveals three candidate residues for this specificity (Fig. 4C). Phe<sup>682</sup> replaces a serine in most PKS and bacterial homologs, whereas Phe<sup>553</sup> and Met<sup>499</sup> substitute for conserved glutamine residues. Together, these three substitutions create a considerably more hydrophobic active site. The two phenylalanines form a hydrophobic cavity, which may allow Met<sup>499</sup> to flip onto the methyl group of an acetyl substrate. Thus, the dual specificity of mFAS MAT appears to result from the combined presence of the conserved arginine for salt-bridging malonyl substrates and the more hydrophobic nature of the active site. The double specificity can be changed by mutating the arginine to alanine,

which then transforms the MAT into an acetyl transferase (34).

**Ketoreductase.** The NADPH-dependent KR domain belongs to the family of short-chain dehydrogenases/reductases (SDRs) (35)—single-domain proteins that have a characteristic Rossmann fold and a substrate binding extension inserted before the last helix. mFAS KR is structurally closely related to both the tetrameric bacterial KR (FabG, 2.0 Å RMSD) and ER (FabI, 2.2 Å RMSD) and to the fungal KR domain (2.6 Å RMSD) (table S4). As for the KS and MAT domains, the closest structural homology is observed with the KR domains from modular PKS (RMSDs of 1.5 Å for tylosin PKS KR and 1.6 Å for DEBS KR). The arrangement of residues in the active site of the mFAS KR domain is consistent with a proton-relay mechanism described for bacterial FabG (36). However, two residues of the proton-wire, Asn<sup>2038</sup> and

Lys<sup>1995</sup>, have swapped positions (Fig. 4D), as previously observed in PKS KR domains (19, 20). Loops in the vicinity of the active site cleft are disordered in the apo form of mFAS and become stabilized upon cofactor binding. This includes residues 1975 to 1990, corresponding to the  $\beta_4/\alpha_4$  loop in FabG, that are presumably stabilized by interactions of Met<sup>1973</sup> with the active site Lys<sup>1995</sup>, and part of the substrate binding extension (residues 2072 to 2075). The direction of substrate entry into the active site can be inferred from the stereospecificity of mFAS KR, which produces an *R*-hydroxyl group (6, 20). The substrate approaches the NADPH cofactor from above the nicotinamide ribose, as observed for the structurally related mycobacterial ER InhA (37, 38).

**Dehydratase.** The mFAS DH domain adopts a pseudodimeric double hot dog fold (Fig. 5A). The subdomain arrangement is more similar to

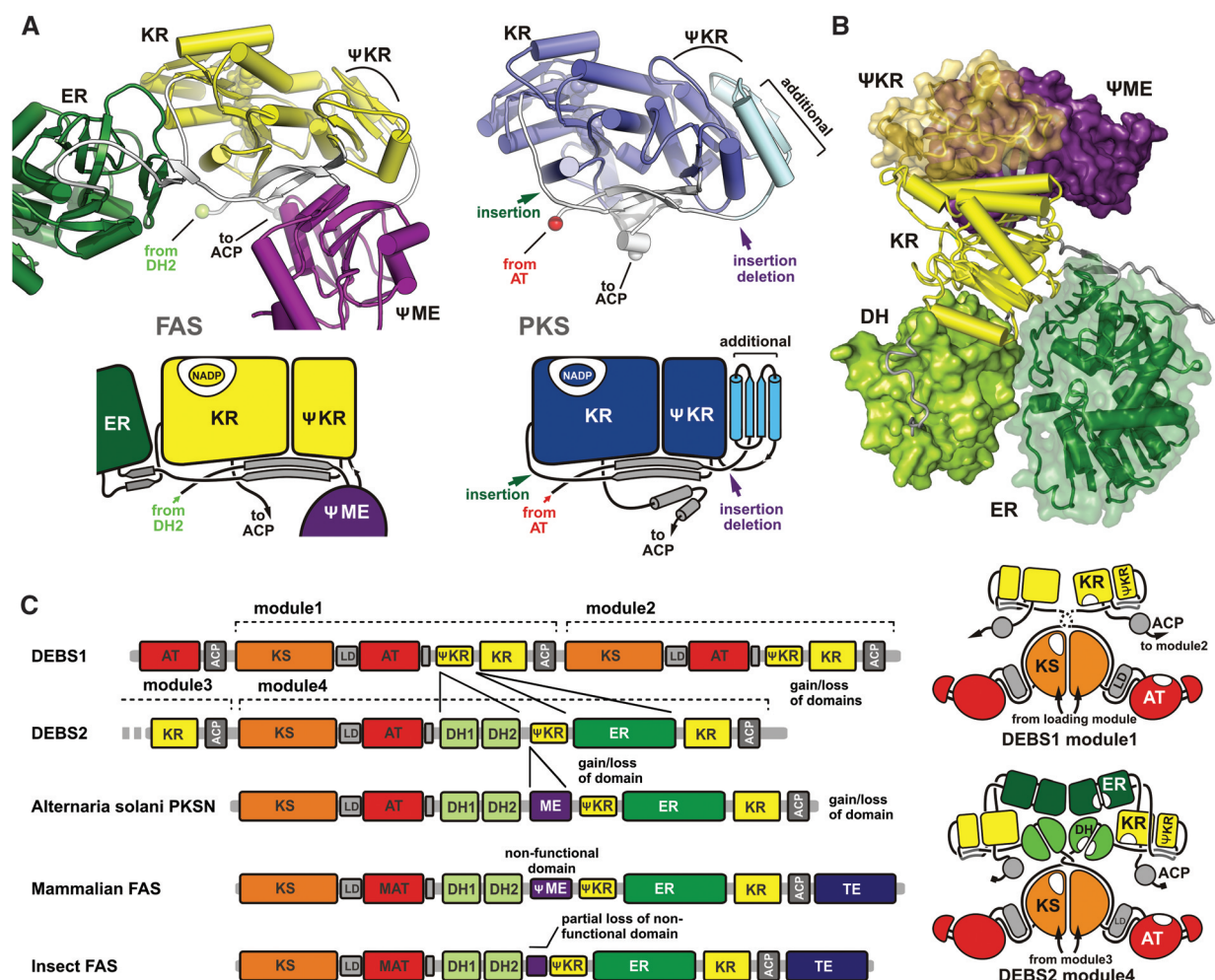


**Fig. 3.** Modularity of the modifying part of mFAS. **(A)** Comparison of the KR/ΨKR arrangement in mFAS (at left) and a related polyketide synthase, DEBS1 (19) (at right). The lower panels provide a schematic overview. The only modifying domain present in DEBS1 PKS includes KR-ΨKR, which is N- and C-terminally extended compared with mFAS KR/ΨKR. The additional ER and DH domains are integrated into mFAS without disturbing the path of the KR/ΨKR linker compared with PKS, leaving the N and C

termini in identical positions. **(B)** KR interacts with all other domains in the modifying part of mFAS, whereas no direct interactions occur between either of the nonenzymatic domains and DH or ER. **(C)** Schematic sequence diagram depicting the integration and removal of additional domains in the modifying parts of PKS, mFAS, and insect FAS, on the basis of structural and sequence alignments (at left). The putative domain topologies of DEBS modules 1 and 4 are shown schematically on the right.

the functional DH dimers of bacterial FabA/Z than to the pseudodimeric fungal DH (fig. S9 and table S4) (39, 40). Each mFAS pseudodimer contains a single composite active site formed by residues His<sup>878</sup> from the N-terminal hot dog fold and Asp<sup>1033</sup> and His<sup>1037</sup> from the C-terminal fold (Fig. 5B). The catalytic importance of these amino acids in mFAS has been demonstrated by mutagenesis and is further corroborated by a topologically similar arrangement in the active centers of bacterial DHs (Fig. 5B) (39–42). This also suggests a similar two-base reaction mechanism, as proposed for *E. coli* FabA, with His<sup>878</sup> and Asp<sup>1033</sup> participating in substrate protonation and deprotonation (39). The histidine at position 1037 is only present in the active site of chicken and pig FAS, whereas in all other sequenced mFAS the corresponding amino acid is a glutamine (fig. S10). The equivalence of a histidine and a glutamine at this position has been verified by mutagenesis (42). In the mFAS structure, His<sup>1037</sup> is positioned toward Asp<sup>1033</sup> at hydrogen-

bonding distance, indicating a stabilizing function similar to those of the glutamine in other mFAS and bacterial DHs (40).

A hydrophobic substrate binding tunnel starts at the pseudodimer interface, stretches through the C-terminal hot dog domain, and has an open end that points toward the top of the FAS assembly (Fig. 5A). In contrast to type II DHs, which harbor two equivalent active sites in each homodimer, the second catalytic site is inactive in mFAS: The loop harboring the second catalytic histidine in bacteria is reduced to a short turn, and the corresponding accessory catalytic residues located in the central helix of the fold are replaced by tryptophane and lysine (Fig. 5A). The hydrophobic tunnel is entirely absent, and the domain is truncated by 30 residues at the N terminus.

**Enoylreductase.** In contrast to all other functional domains of the fatty acid elongation cycle, the mFAS ER has a different fold from its functional analogs in the bacterial type II FAS

system, where the ERs are either SDR [FabI, FabL, FabV (43–45)] or TIM barrel proteins (FabK)—the latter also found as an ER domain in fungal type I FAS (2, 46). Instead, the mammalian ER establishes a subfamily of medium-chain dehydrogenases/reductases (MDRs) (47) that is structurally related to bacterial quinone oxidoreductase (table S4). The mFAS ER contains two subdomains, a nucleotide binding Rossmann-fold (residues 1651 to 1794) and a substrate binding portion (residues 1530 to 1650 and 1795 to 1858). It binds the NADP<sup>+</sup> cofactor in an open extended conformation between the two subdomains (Fig. 5C). Our structure identifies Lys<sup>1771</sup> and Asp<sup>1797</sup> as candidate donor residues for substrate protonation after hydride transfer from NADPH (Fig. 5D). These two residues are in close proximity to the hydride-donating nicotinamide C4, in a similar position as the suggested active site tyrosines in other MDR subfamilies (e.g., the mitochondrial ER) (48–50). The two residues are strictly conserved in mFAS (fig. S11), and a corresponding lysine/aspartate pair is observed in the apo-form structure of the nucleotide binding subdomain of a related type I PKS ER domain (PDB entry 1pqw). The active site of ER is located in a narrow crevice created in part by the bound nucleotide cofactor, very different from the substrate binding groove in the related quinone reductase (50). Substrate entry probably occurs through a tunnel along the cofactor toward the nicotinamide ring. The tunnel continues through a constriction toward the back of the ER domain, where an opening would allow exit of long acyl chains (Fig. 5C).

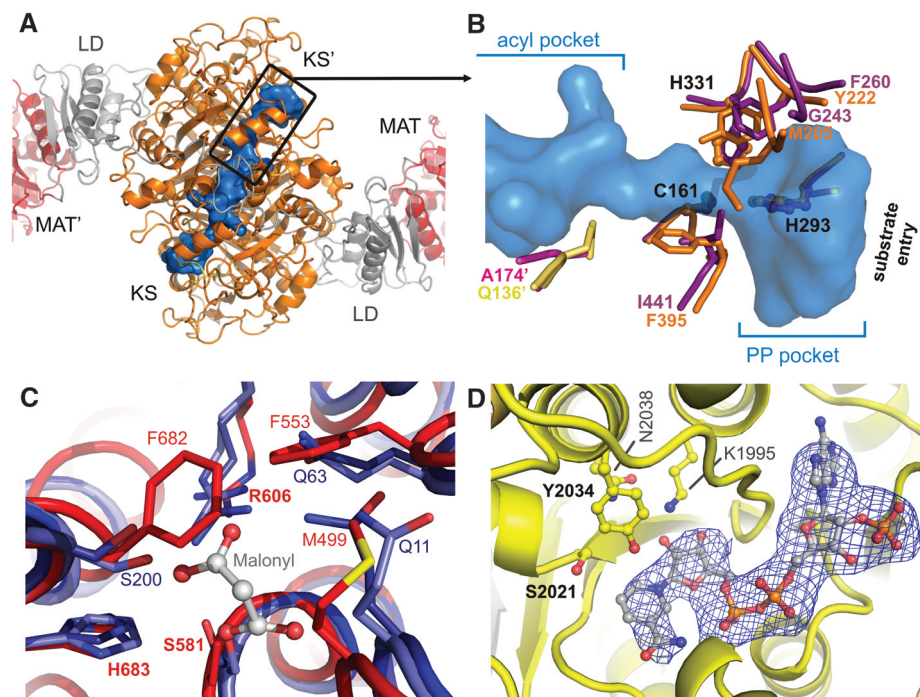


**Fig. 4.** Active sites of KS, MAT, and KR. **(A)** A large substrate binding tunnel (blue surface representation) traverses the dimeric KS domain. The substrate entry site of the KS domains is oriented toward the MAT domain of the other chain. **(B)** A narrow constriction in the substrate binding tunnel of the KS domain adjacent to the conserved active site residues (labeled in black) prevents the entry of larger modified substrates. Four residues involved in the formation of the constriction (orange for one subunit and yellow for the second one) are conserved in mFAS and replaced with smaller residues in the more permissive KS domains of PKS, as exemplified by KS of DEBS module 5 (purple for one subunit and pink for the second) (18). **(C)** MAT active site of mFAS (red) compared to bacterial MT, with and without bound substrate (light and dark blue, respectively) (32, 33). Conserved active site residues in mFAS are indicated in bold. Two phenylalanines and a methionine characteristic for the acetyl-CoA/malonyl-CoA double-specific mFAS create a more hydrophobic binding groove and may close onto the methyl group of an acetyl moiety to promote efficient binding. **(D)** Active site of KR with bound NADP<sup>+</sup> and a 3.3 Å unbiased simulated annealed omit electron density map for the cofactor, contoured at 2.7 $\sigma$ . The proton-donating tyrosine is in equivalent position to bacterial homologs, but the asparagine (N<sup>2038</sup>) and lysine (K<sup>1995</sup>) involved in proton replenishment are swapped.

### Structural Relation to PKS

The structural information presented here provides extensive evidence for the evolutionary relationship between mFAS and bacterial and fungal PKSs. (i) All catalytic mFAS domains are most closely related to PKS domains at the sequence level. Notably, the domains of mFAS are more similar to PKS domains than to the bacterial FAS counterparts, despite the differences in their substrate specificities. (ii) The structure of mFAS demonstrates that the similarity to PKSs extends to the linkers and the overall architecture—e.g., those in the KS/MAT or the KR/ $\Psi$ KR regions—despite very low sequence conservation. (iii) Finally, an additional piece of evidence is provided by the existence of the nonfunctional  $\Psi$ ME domain, which can be considered a remnant of a catalytically active domain present in a common evolutionary ancestor of mFAS and PKS that is still preserved in several PKSs (28–30).

Functionally, modular PKSs differ from FAS by their non-iterative mode of action, where each module carries out a single precursor elongation step equivalent to one round of chain elongation by mFAS (51). The modules are concatenated into large polypeptides, several of which may assemble into production lines with more than 10 modules. This allows the synthesis of a variety of structurally diverse compounds. Based on the

structural similarity discussed above, mFAS can be considered as a single PKS module specialized for iterative fatty acid synthesis.

Individual PKS modules contain substrate loading and condensing domains and variations of domains involved in  $\beta$ -carbon processing that control the chemical structure of the produced polyketide. Overall comparison of the PKS DEBS module 1 KR- $\Psi$ KR, which is the only  $\beta$ -carbon-modifying domain in this module, with the corresponding parts of mFAS reveals the structural basis for the notable modularity of modifying domains in megasynthases: Mediated by short linking sequences emanating from conserved secondary structure elements, the full ER domain is inserted between the  $\Psi$ KR and KR domain, whereas the  $\Psi$ ME domain is integrated into the linker leading into the N terminus of the  $\Psi$ KR domain (Fig. 3, A and C). As a consequence of this architectural solution, the insertions do not affect the core folds of the  $\Psi$ KR and KR domains. Furthermore, because of a very flexible mode of interaction between KS and DH and weak contacts between KR and either DH or ER (table S3) of the mFAS, it is relatively easy to envision the architecture of some representative PKS modules (Fig. 3C). For example, the minimal PKS module, such as module 1 of DEBS1, which includes only the KR of the possible  $\beta$ -carbon-processing domains, would have this domain linked to KS with a short 10-amino acid linker, similar to the linker connecting KS to DH in mFAS. Other truncated variants of the mFAS architecture are also detectable at the sequence level. In the case of the closely related insect FAS, the  $\Psi$ ME domain lacks the N-terminal extension (Fig. 3C and fig. S8), whereas there is no methyltransferase in DEBS module 4 (Fig. 3C) (19, 52). Short extensions may substitute for missing domain interactions, as indicated by a C-terminal addition of two helices to the KR- $\Psi$ KR of DEBS 1 (19) (Fig. 3A), which covers the region of the  $\Psi$ KR surface occupied by the  $\Psi$ ME in mFAS.

These results also imply that the iterative mode of elongation (in which ACP shuttles substrates within one module) and a noniterative elongation (where substrates are passed between modules) can be accomplished with a similar overall architecture of the molecules. Notably, compared to the mFAS structure, no supplementary elements with a potential role in oligomerization are observed in the PKS structures available so far, except for a single helix in the KS-MAT linker domain (fig. S1) and a small C-terminal extension of the KR domain (Fig. 3A). Apparently, the N- and C-terminal docking domains (53, 54) are sufficient to determine the higher-order assembly of PKS modules and polypeptides.

The architecture and the fold of mFAS and of the related PKSs are extremely versatile. This is in contrast to fungal FAS, which forms a barrel-shaped 2.6 MD  $\alpha_6\beta_6$ -heterododecameric assembly with three full sets of active sites enclosed in

each of the two reaction chambers (2, 13). The scaffold of the cage-forming fungal FAS appears less tolerant toward product modifying domain insertions and excisions because of symmetry constraints and the tight embedding of catalytic domains. Consistently, no naturally occurring fungal type I FAS with an altered domain composition has been detected, and all fungal FAS and most of their homologs produce only saturated fatty acid products (8).

### Substrate Shuttling by the ACP Domain

The entry sites to the active centers of the mFAS enzymatic domains are grouped around the two lateral clefts. In each cleft, the entry sites of MAT, DH, and ER are oriented toward one face of mFAS, and those of KS and KR toward the other face (Fig. 6). The flexibly tethered ACP and the following TE domains are not visualized in the structure. However, the structure defines the anchor point of ACP at residue 2113 in the center of the upper portion of the lateral clefts of mFAS. Together with recent structures of closely related rat and human ACP (14, 15), which

define the first ordered ACP residue at positions 2125 to 2127 (porcine FAS numbering), the flexible KR-ACP linker is composed of 12 to 14 amino acids, corresponding to a maximum length of  $\sim 40$  Å. With a length of 23 to 26 residues, the ACP-TE linker is substantially longer and could span up to an 80 Å distance, as deduced from the corresponding isolated domain structures (14–17). In contrast to the fungal ACP linkers, which have a high Pro/Ala content that can increase their stiffness (55), the tethers flanking mFAS ACP have no unusual amino acid composition (Fig. 6). Whereas the motion of fungal ACP is constrained by double-tethering, no second anchor point is apparent for mFAS ACP, because the subsequent TE domain is not located at a defined position relative to the body of mFAS. Still, the TE domain may influence the motion of the tethered ACP either by transiently interacting with other domains or by steric effects.

Confining the path of the ACP may be one role of the protruding noncatalytic  $\Psi$ ME domain. This domain is docked to the body of mFAS in the vicinity of the ACP anchor point (Fig. 1, A

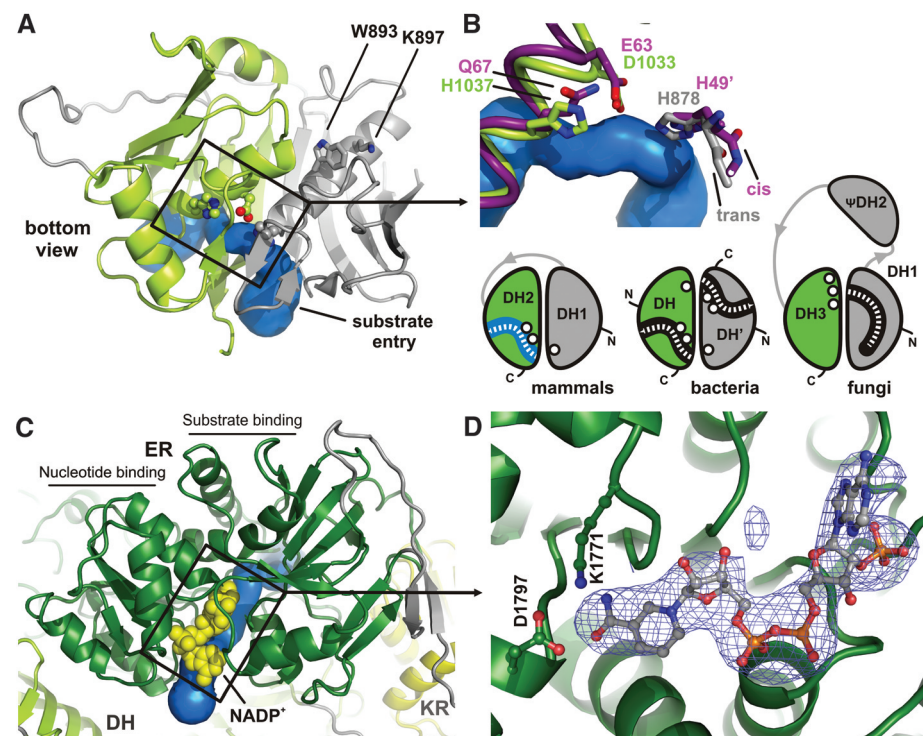


**Fig. 5.** Active sites of DH and ER. (A) Pseudo-dimeric DH domain only harbors a single active site and substrate binding tunnel with an open end. Active site residues are shown in ball-and-stick representation. These residues are not conserved in the corresponding position of the second subdomain (Trp<sup>893</sup> and Lys<sup>897</sup>). (B) Close-up view of the DH active site topology (top) and schematic comparison to bacterial and fungal FAS (bottom). The mFAS active site residues (green) have their functional groups in similar positions as their bacterial FabZ counterparts (40) (purple), despite the exchange of two amino acids and the loss of an unusual non-proline cis peptide bond at H<sup>878</sup>. (C) Open-ended substrate binding tunnel (blue) of the ER domain of mFAS shown in the presence of the bound NADP<sup>+</sup> cofactor (yellow spheres). (D) Two amino acids, Asp<sup>1797</sup> and Lys<sup>1771</sup>, are candidate proton donor residues for enoyl reduction based on the positioning of their functional groups at  $\sim 4.2$  Å distance to the C4 of the NADP<sup>+</sup> nicotinamide ring. A 3.3 Å unbiased simulated annealed omit electron density map for the bound NADP<sup>+</sup> cofactor, contoured at 3.3 $\sigma$ , is shown.

and B) and narrows the accessible region along the MAT, KS, DH, and ER substrate entry sites to a rim that is just slightly wider than the ACP (Fig. 6 and fig. S7C). The discrete ACPs of bacterial-type FAS (56–58) sequester fully saturated fatty acyl chains within their hydrophobic core. In contrast, mFAS ACP does not bury the acyl chain inside its core (14), raising the question whether other parts of the molecule may have taken over this function (for instance, by providing hydrophobic rims for a sliding motion of ACP-tethered acyl chains on the surface of mFAS). However, mapping of conservation or electrostatic potential on the mFAS surface did not reveal such regions.

The linker length, together with the steric constraints of the mFAS structure, allows ACP to reach a full set of active sites in one cleft but no active sites from the other cleft. During the elongation cycle (Fig. 6), the ACP is first loaded with substrates at the lateral MAT domain. ACP then has to deliver the substrates to the KS entry

pocket on the opposite face of mFAS. The shortest route would lead directly through the cleft (path 1 in Fig. 6), which is just sufficiently open to allow the passage of ACP. After condensation at the KS, the ACP must reach the KR on the same face as the KS active site (path 2) before crossing the cleft again to approach the DH domain (path 3). From here, ACP proceeds toward the nearby ER (path 4) and finally delivers the fully saturated substrate to the KS active center before being reloaded at the MAT for the next cycle. During this cycle, the ACP interacts with the MAT and the  $\beta$ -carbon-processing domains of one chain, but it also interacts with the KS of the second polypeptide chain in the FAS dimer. Notably, the partially preserved active site cleft of the catalytically inactive  $\Psi$ ME domain could easily be accessed by ACP from the reaction chamber, as required in PKSs that display methyltransferase activity (fig. S7C) (28, 30).

The requirement for ACP to shuttle back and forth through the cleft does not appear to be the most favorable solution for efficient substrate transfer and catalysis by mFAS. An alternative is suggested by considering the properties of the junction between the lower condensing and the upper modifying part of mFAS: They are joined only via the MAT-DH linkers, which are expected to mediate a flexible junction between the two halves of  $\sim 200$  kD molecular mass each (59). Moreover, the pseudosymmetry-related DH/KS contacts on either side of the joint are not identical as would be expected for a stable interaction in solution. Consequently, the flexible connection of the mFAS halves may allow rotational motion around the dimer axis or a certain degree of tilting. Such motion would drag the ACP between the two faces of FAS and may contribute considerably to productive substrate shuttling. Mutant complementation and cross-linking studies have demonstrated that the vast majority of sub-

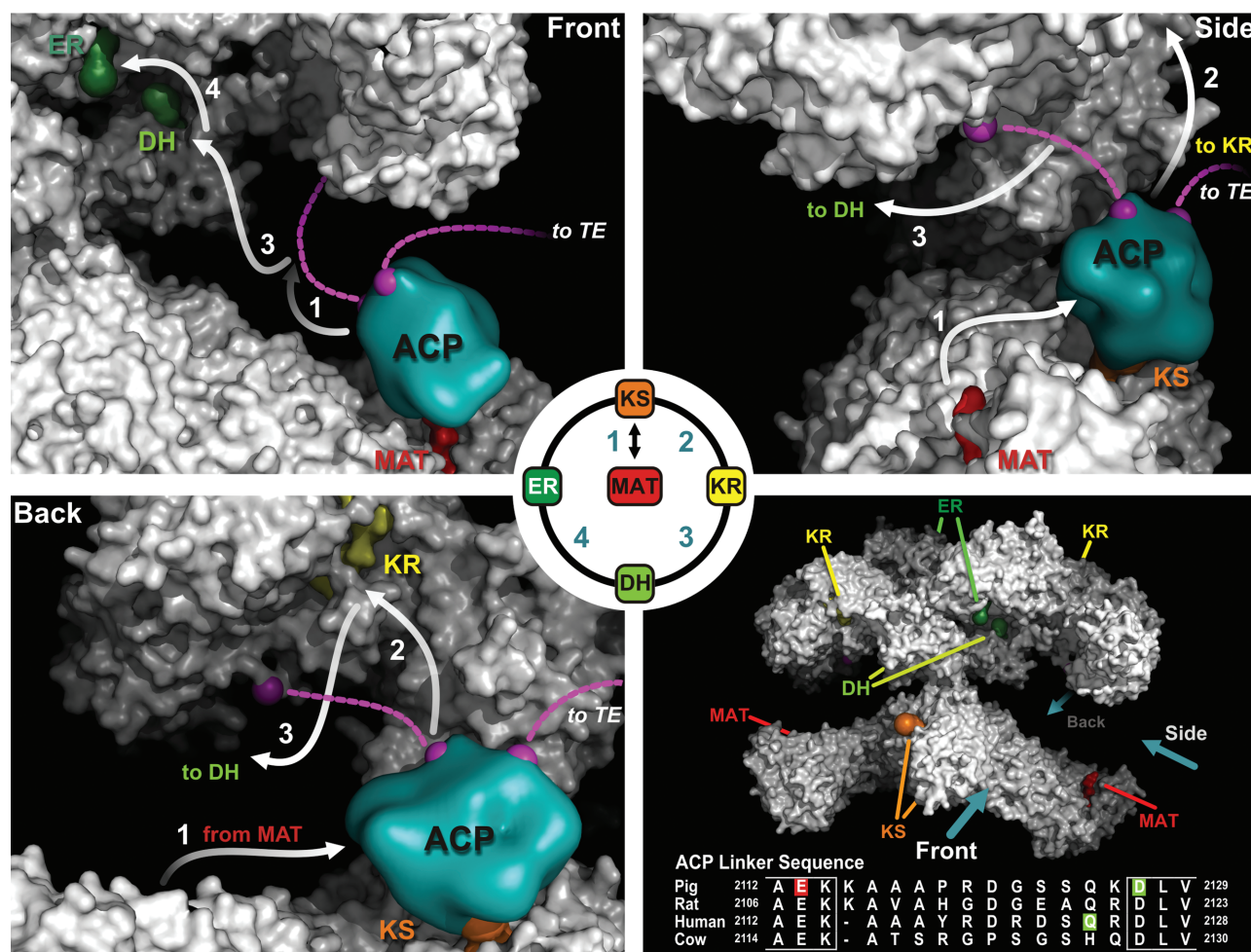


**Fig. 6.** Substrate shuttling by the ACP in mFAS. After substrate loading at the MAT on one side of the reaction chamber, the flexibly linked ACP has to shuttle the substrates to the other side for condensation at the KS and reduction at the KR (paths 1 and 2). To reach the DH and ER domain, ACP has to cross the cleft a second time (paths 3 and 4) before the saturated acyl chain can be back-transferred to KS to serve as primer for the next elongation cycle. The flexible linkers of ACP are depicted by dashed lines

(pink). The precise length of the KR-ACP linker is defined by the KR and ACP domain borders in the current and previously solved structures (14, 16, 17) (bottom right, red and green). A schematic representation of the mFAS ACP domain based on experimentally determined structures (14, 15) was positioned to the active site clefts by superposition with fungal ACP bound to the KS domain (13) and by orienting it according to residual electron density observed in the active site cleft of MAT (fig. S12).

strates are processed in mFAS by individual full sets of active sites, according to the path of ACP described above. However, these studies have also shown that a minority of substrates can be shuttled between the two sets of active sites, either by ACP serving both MAT domains or by direct interaction of ACP with both KS domains (6, 60–62). In light of the large 135 Å distance between the ACP anchor point located in one catalytic cleft and the MAT in the other, the most plausible explanation for the minor mode-of-domain interaction is a large-scale rotation of the upper portion of mFAS, relative to the lower portion (fig. S4).

The molecular description of active sites in mFAS should stimulate the development of improved inhibitors as anticancer drug candidates. As demonstrated by structural homology, this structure is also a good template for the organization of PKS modules; it agrees with and extends present theoretical models of PKS architecture (19, 22). Furthermore, the structure of mFAS paves the way for structure-based experiments to answer remaining questions on the dynamics and substrate shuttling mechanism in megasynthases.

#### References and Notes

1. S. W. White, J. Zheng, Y. M. Zhang, C. O. Rock, *Annu. Rev. Biochem.* **74**, 791 (2005).
2. S. Jenni *et al.*, *Science* **316**, 254 (2007).
3. S. Jenni, M. Leibundgut, T. Maier, N. Ban, *Science* **311**, 1263 (2006).
4. I. B. Lomakin, Y. Xiong, T. A. Steitz, *Cell* **129**, 319 (2007).
5. T. Maier, S. Jenni, N. Ban, *Science* **311**, 1258 (2006).
6. S. Smith, S. C. Tsai, *Nat. Prod. Rep.* **24**, 1041 (2007).
7. F. Lynen, *Eur. J. Biochem.* **112**, 431 (1980).
8. E. Schweizer, J. Hofmann, *Microbiol. Mol. Biol. Rev.* **68**, 501 (2004).
9. F. P. Kuhajda *et al.*, *Proc. Natl. Acad. Sci. U.S.A.* **91**, 6379 (1994).
10. J. A. Menendez, R. Lupu, *Nat. Rev. Cancer* **7**, 763 (2007).
11. F. P. Kuhajda, *Cancer Res.* **66**, 5977 (2006).
12. H. Orita *et al.*, *Clin. Cancer Res.* **13**, 7139 (2007).
13. M. Leibundgut, S. Jenni, C. Frick, N. Ban, *Science* **316**, 288 (2007).
14. E. Ploskon *et al.*, *J. Biol. Chem.* **283**, 518 (2008).
15. G. Bunkoczi *et al.*, *Chem. Biol.* **14**, 1243 (2007).
16. B. Chakravarty, Z. Gu, S. S. Chirala, S. J. Wakil, F. A. Quiocho, *Proc. Natl. Acad. Sci. U.S.A.* **101**, 15567 (2004).
17. C. W. Pemble IV, L. C. Johnson, S. J. Kridel, W. T. Lowther, *Nat. Struct. Mol. Biol.* **14**, 704 (2007).
18. Y. Tang, C.-Y. Kim, I. I. Mathews, D. E. Cane, C. Khosla, *Proc. Natl. Acad. Sci. U.S.A.* **103**, 11124 (2006).
19. A. T. Keatinge-Clay, R. M. Stroud, *Structure* **14**, 737 (2006).
20. A. T. Keatinge-Clay, *Chem. Biol.* **14**, 898 (2007).
21. Y. Tang, A. Y. Chen, C.-Y. Kim, D. E. Cane, C. Khosla, *Chem. Biol.* **14**, 931 (2007).
22. C. Khosla, Y. Tang, A. Y. Chen, N. A. Schnarr, D. E. Cane, *Annu. Rev. Biochem.* **76**, 195 (2007).
23. A. K. Joshi, A. Witkowski, H. A. Berman, L. Zhang, S. Smith, *Biochemistry* **44**, 4100 (2005).
24. Materials and methods are available as supporting material on Science Online.
25. J. G. Olsen, A. Kadziola, P. von Wettstein-Knowles, M. Siggaard-Andersen, S. Larsen, *Structure* **9**, 233 (2001).
26. J. M. Thorn, J. D. Barton, N. E. Dixon, D. L. Ollis, K. J. Edwards, *J. Mol. Biol.* **249**, 785 (1995).
27. J. L. Martin, F. M. McMillan, *Curr. Opin. Struct. Biol.* **12**, 783 (2002).
28. I. Fujii, N. Yoshida, S. Shimomaki, H. Oikawa, Y. Ebizuka, *Chem. Biol.* **12**, 1301 (2005).

29. I. Molnar *et al.*, *Chem. Biol.* **7**, 97 (2000).
30. D. J. Edwards *et al.*, *Chem. Biol.* **11**, 817 (2004).
31. A. Witkowski, A. K. Joshi, S. Smith, *Biochemistry* **36**, 16338 (1997).
32. L. Serre, E. C. Verbree, Z. Dauter, A. R. Stuitje, Z. S. Derewenda, *J. Biol. Chem.* **270**, 12961 (1995).
33. C. Oefner, H. Schulz, A. D'Arcy, G. E. Dale, *Acta Crystallogr. D Biol. Crystallogr.* **62**, 613 (2006).
34. V. S. Rangan, S. Smith, *J. Biol. Chem.* **272**, 11975 (1997).
35. B. Persson, Y. Kallberg, U. Oppermann, H. Jornvall, *Chem. Biol. Interact.* **143–144**, 271 (2003).
36. A. C. Price, Y. M. Zhang, C. O. Rock, S. W. White, *Structure* **12**, 417 (2004).
37. D. A. Rozwarski, C. Vilcheze, M. Sugantino, R. Bittman, J. C. Sacchettini, *J. Biol. Chem.* **274**, 15582 (1999).
38. T. J. Sullivan *et al.*, *Am. Chem. Soc. Chem. Biol.* **1**, 43 (2006).
39. M. Leesong, B. S. Henderson, J. R. Gillig, J. M. Schwab, J. L. Smith, *Structure* **4**, 253 (1996).
40. M. S. Kimber *et al.*, *J. Biol. Chem.* **279**, 52593 (2004).
41. A. K. Joshi, S. Smith, *J. Biol. Chem.* **268**, 22508 (1993).
42. S. Pasta, A. Witkowski, A. K. Joshi, S. Smith, *Chem. Biol.* **14**, 1377 (2007).
43. C. Baldock, J. B. Rafferty, A. R. Stuitje, A. R. Slabas, D. W. Rice, *J. Mol. Biol.* **284**, 1529 (1998).
44. R. J. Heath, N. Su, C. K. Murphy, C. O. Rock, *J. Biol. Chem.* **275**, 40128 (2000).
45. R. P. Massengo-Tiasse, J. E. Cronan, *J. Biol. Chem.* **283**, 1308 (2008).
46. J. Saito *et al.*, *Protein Sci.* **17**, 691 (2008).
47. E. Nordling, H. Jornvall, B. Persson, *Eur. J. Biochem.* **269**, 4267 (2002).
48. T. T. Airene *et al.*, *J. Mol. Biol.* **327**, 47 (2003).
49. T. Hori *et al.*, *J. Biol. Chem.* **279**, 22615 (2004).
50. Y. Shimomura, Y. Kakuta, K. Fukuyama, *J. Bacteriol.* **185**, 4211 (2003).
51. D. A. Hopwood, D. H. Sherman, *Annu. Rev. Genet.* **24**, 37 (1990).
52. C. D. Richter *et al.*, *FEBS J.* **274**, 2196 (2007).
53. C. D. Richter, D. Nietlisbach, R. W. Broadhurst, K. J. Weissman, *Nat. Chem. Biol.* **4**, 75 (2008).
54. K. J. Weissman, *ChemBioChem* **7**, 485 (2006).
55. R. N. Perham, *Biochemistry* **30**, 8501 (1991).
56. A. Roujeinikova *et al.*, *Structure* **10**, 825 (2002).
57. A. Roujeinikova *et al.*, *J. Mol. Biol.* **365**, 135 (2007).
58. G. A. Zornetzer, B. G. Fox, J. L. Markley, *Biochemistry* **45**, 5217 (2006).
59. S. Jones, J. M. Thornton, *Proc. Natl. Acad. Sci. U.S.A.* **93**, 13 (1996).
60. S. Smith, A. Witkowski, A. K. Joshi, *Prog. Lipid Res.* **42**, 289 (2003).
61. A. K. Joshi, V. S. Rangan, A. Witkowski, S. Smith, *Chem. Biol.* **10**, 169 (2003).
62. V. S. Rangan, A. K. Joshi, S. Smith, *Biochemistry* **40**, 10792 (2001).
63. All data were collected at the Swiss Light Source (SLS, Paul Scherrer Institute, Villigen). We thank C. Schulze-Briese, S. Gutmann, R. Bingel-Erlenmeyer, S. Russo, A. Pauluhn, and T. Tomizaki for their outstanding support at the SLS; S. Jenni and M. Sutter for critically reading the manuscript and all members of the Ban laboratory for suggestions and discussions; R. Grosse-Kunstleve, P. Afonine, and P. Adams for support with the PHENIX software; and A. Jones for support with the program O. This work was supported by the Swiss National Science Foundation (SNSF) and the National Center of Excellence in Research Structural Biology program of the SNSF. Structure factors and atomic coordinates of the porcine FAS in the apo- and NADP<sup>+</sup>-bound form have been deposited in the Protein Data Bank with accession codes 2zv8 and 2zv9.

#### Supporting Online Material

www.sciencemag.org/cgi/content/full/321/5894/1315/DC1  
Materials and Methods  
Figs. S1 to S15  
Tables S1 to S4  
References

3 June 2008; accepted 31 July 2008  
10.1126/science.1161269

## Internally Generated Cell Assembly Sequences in the Rat Hippocampus

Eva Pastalkova, Vladimir Itskov,\* Asohan Amarasingham, György Buzsáki†

A long-standing conjecture in neuroscience is that aspects of cognition depend on the brain's ability to self-generate sequential neuronal activity. We found that reliably and continually changing cell assemblies in the rat hippocampus appeared not only during spatial navigation but also in the absence of changing environmental or body-derived inputs. During the delay period of a memory task, each moment in time was characterized by the activity of a particular assembly of neurons. Identical initial conditions triggered a similar assembly sequence, whereas different conditions gave rise to different sequences, thereby predicting behavioral choices, including errors. Such sequences were not formed in control (nonmemory) tasks. We hypothesize that neuronal representations, evolved for encoding distance in spatial navigation, also support episodic recall and the planning of action sequences.

A prominent theory states that the hippocampal system primarily serves spatial navigation (1, 2); a component of this theory is that the place-dependent activity of neurons [place cells (1, 2)] in the hippocampus arises from external serially ordered environmental stimuli (3–7). Place cells are thought to embody the representation of a cognitive map, enabling flexible navigation. However, neural theories of other cognitive processes that may depend on the hippocampus, such as episodic

memory and action planning, draw on the activity of hypothetical internally organized cell assemblies (8–13).

Center for Molecular and Behavioral Neuroscience, Rutgers, The State University of New Jersey, 197 University Avenue, Newark, NJ 07102, USA.

\*Present address: Center for Neurobiology and Behavior, Columbia University, 1051 Riverside Drive, New York, NY 10032, USA.

†To whom correspondence should be addressed. E-mail: buzsaaki@axon.rutgers.edu



**The Crystal Structure of a Mammalian Fatty Acid Synthase**  
Timm Maier, Marc Leibundgut and Nenad Ban (September 5, 2008)

*Science* **321** (5894), 1315-1322. [doi: 10.1126/science.1161269]

Editor's Summary

---

This copy is for your personal, non-commercial use only.

---

- Article Tools** Visit the online version of this article to access the personalization and article tools:  
<http://science.sciencemag.org/content/321/5894/1315>
- Permissions** Obtain information about reproducing this article:  
<http://www.sciencemag.org/about/permissions.dtl>

*Science* (print ISSN 0036-8075; online ISSN 1095-9203) is published weekly, except the last week in December, by the American Association for the Advancement of Science, 1200 New York Avenue NW, Washington, DC 20005. Copyright 2016 by the American Association for the Advancement of Science; all rights reserved. The title *Science* is a registered trademark of AAAS.